



# Microwave-assisted microemulsion synthesis of carbon supported Pt-WO<sub>3</sub> nanoparticles as an electrocatalyst for methanol oxidation

Chunzhen Yang<sup>a</sup>, Nicole K. van der Laak<sup>a,b,\*</sup>, Kwong-Yu Chan<sup>a,\*\*</sup>, Xin Zhang<sup>c</sup>

<sup>a</sup> Department of Chemistry, The University of Hong Kong, Pokfulam Road, Hong Kong

<sup>b</sup> Department of Chemistry, Centre for Advanced Energy Storage and Recovery (CAESAR), Herriot-Watt University, Edinburgh EH14 4AS, United Kingdom

<sup>c</sup> Department of Chemistry, Shantou University, China

## ARTICLE INFO

### Article history:

Received 9 November 2011

Received in revised form 25 April 2012

Accepted 28 April 2012

Available online 6 May 2012

### Keywords:

Pt-WO<sub>3</sub> nanoparticles

Microwave

Microemulsion

Methanol oxidation

Cu-UPD

## ABSTRACT

A microwave-assisted microemulsion synthesis of carbon supported Pt-WO<sub>3</sub> nanoparticles is presented. Amorphous WO<sub>3</sub> nanoparticles of 1.0 nm in size were first deposited onto carbon from an alkaline tungstate containing microemulsion *via* mixing with an acid containing microemulsion under controlled microwave exposure. Platinum was subsequently deposited onto the carbon supported WO<sub>3</sub> nanoparticles by reducing H<sub>2</sub>PtCl<sub>6</sub> in a microemulsion under controlled microwave exposure forming nanoparticles with an average size of 2.5 nm. This method produced a homogeneous distribution of nanoparticles on the carbon support with a uniform Pt:W ratio. The Pt:W can be well controlled by varying the metal precursors' Pt:W ratio. Hydrogen adsorption, CO-stripping and Cu-UPD stripping method were used to estimate the electrochemical surface area of Pt in the Pt-WO<sub>3</sub> mixed catalyst system. Cyclic voltammetry and chronopotentiometry experiments demonstrate that a 1:1 ratio of Pt:W has the highest electrocatalytic activity based on Pt mass for methanol oxidation in sulfuric acid. The enhanced electrocatalytic activity is attributed to both physical and chemical influence of the WO<sub>3</sub> component.

© 2012 Elsevier Ltd. All rights reserved.

## 1. Introduction

The interest in developing fuel cells for high energy density applications, in particular in long-range transportation continues to grow. Platinum has been the most effective electrocatalyst for anodic oxidation of fuels at low temperature, but the commonly generated CO intermediate seriously undermines the catalytic activity of platinum. The development of CO-tolerant electrocatalysts and the lowering of Pt loading for cost-effectiveness are some of the critical issues facing commercialization of fuel cells [1–3]. The addition of a second or third metal has demonstrated to be effective in increasing performance as a function of Pt loading, as well as improving the resistance to CO poisoning. According to the bi-functional mechanism, the CO intermediate formed on the Pt sites can be oxidized by an oxygen-containing species on the neighbouring co-catalyst metal [4,5]. Binary and ternary platinum-based alloys such as Pt–Ru [6,7], Pt–Mo [8,9], Pt–Bi [10], Pt–Co [11,12], Pt–Mn [12], and Pt–Ru–M [13–15], and metal oxides, including RuO<sub>2</sub> [16], TiO<sub>2</sub> [17,18], CeO<sub>2</sub> [19,20], MoO<sub>x</sub> [21,22], SnO<sub>2</sub> [23] and WO<sub>3</sub> [24–28] have been studied to improve stability and CO tolerance

for methanol electro-oxidation. Among these, Pt–Ru bimetallic catalysts dispersed on carbon supports show the best performance. As a precious metal, however, ruthenium is as expensive as Pt and does not help to reduce production costs in scaled commercial applications. A promising cost-effective alternative to Ru is WO<sub>3</sub>, which has been extensively studied for promoting the electrocatalytic activity of Pt. The costs saving effectiveness, however, should be compared in terms of both current and voltage output. Tseung's group demonstrated the hydrogen spill-over effect [29–32] for typical fuel cell anode reactions on Pt/WO<sub>3</sub> electrocatalyst when WO<sub>3</sub> forms a conducting, blue hydrogen tungsten bronze, H<sub>x</sub>WO<sub>3</sub>, when receiving protons in acidic media at the potential region of 0–0.55 V vs. RHE, as shown in the reaction.



The formation of H<sub>x</sub>WO<sub>3</sub> effectively enhances the dehydrogenation step of in a fuel cell anode reaction such as methanol oxidation [29–32]. In addition, OH groups adsorbed on the WO<sub>3</sub> surface may help to oxidize the CO intermediate formed on the Pt site [29], giving the bi-functional catalyst characteristics [30,33–38].

Understanding the structural and compositional effects of Pt-WO<sub>3</sub> on electrocatalysis has been hindered by our ability to synthesize nanoparticles with good control over particle size and the Pt:W ratio. Typically Pt nanoparticles are supported on a WO<sub>3</sub> support by, for example, reducing a platinum precursor

\* Corresponding author.

\*\* Corresponding author at: Department of Chemistry, The University of Hong Kong, Pokfulam Road, Hong Kong.

E-mail address: [n.vanderlaak@gatesscholar.org](mailto:n.vanderlaak@gatesscholar.org) (N.K. van der Laak).

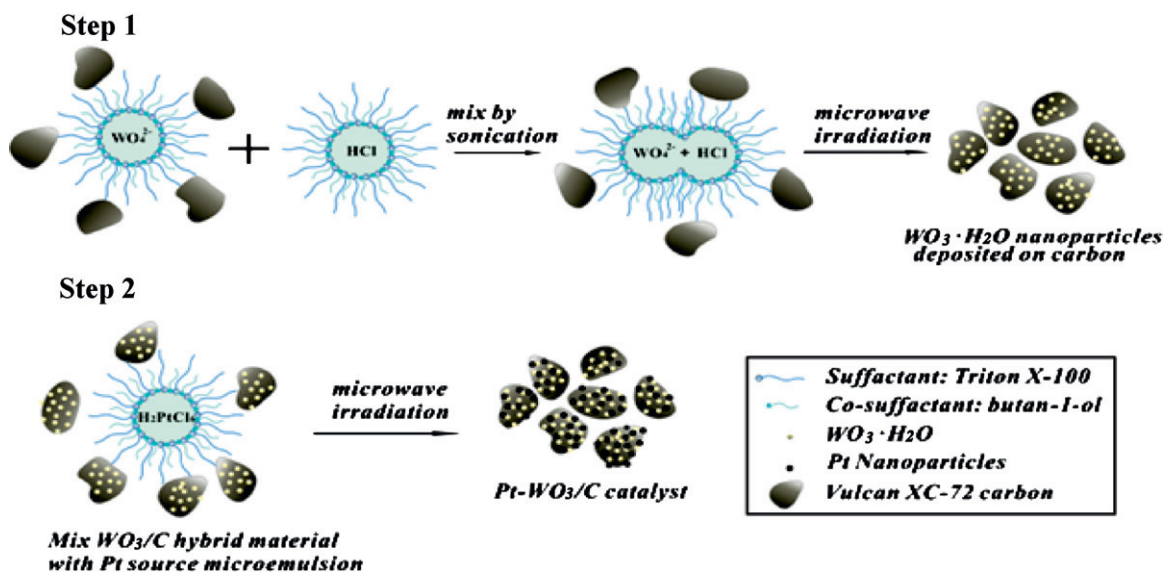


Fig. 1. The preparation process of making Pt-WO<sub>3</sub>/C electrocatalysts through microwave-assisted microemulsion.

onto commercial monoclinic tungsten oxide powder [33,39,40] or by precipitating Pt nanoparticles onto mesoporous WO<sub>3</sub> [25,41]. Other morphologies of tungsten oxide such as nanotubes [42] and nanorods [43,44], have also been prepared and used as supports for platinum. While these Pt/WO<sub>3</sub> composites show high CO tolerance and electrochemical activity comparable to commercial PtRu/C as an anode catalyst, the Pt:W ratio is not controlled and tungsten oxide is normally in excess. The effects of Pt:W ratio, size and structure of WO<sub>3</sub> on the electroactivity cannot be clarified in studies that contain excess WO<sub>3</sub>.

While syntheses of Pt nanoparticles have been well reported, the synthesis of Pt-WO<sub>3</sub> with control of the Pt:W ratio at the nanoparticle level has been difficult. Platinum is usually deposited by chemical reduction while WO<sub>3</sub> is typically deposited from tungstate, the deposition of which is induced by a pH change according to the reaction  $\text{WO}_4^{2-} + 2\text{H}^+ \rightarrow \text{WO}_3 \cdot \text{H}_2\text{O}$ . Controlling the size of the deposited WO<sub>3</sub> nanoparticles in this reaction is problematic. Different methods have been used to prepare WO<sub>3</sub> powders, including electrochemical deposition [45], chemical vapor deposition [46], wet chemical deposition [26], a microemulsion-mediated method [47], a sol-gel method [48], hydrothermal reactions [49], and impregnation [50]. The size of WO<sub>3</sub> particle highly depends on the preparation technique and few of these techniques have reported nanosized WO<sub>3</sub> particles less than 2 nm in diameter. Moreover, the crystallinity and particle morphology changes with increasing particle size. As tungsten oxide has limited electrical conductivity the electroactivity can be adversely affected when WO<sub>3</sub> is present as larger particles. This in turn may affect the promotion of Pt and the ability to remove CO. Some control of WO<sub>3</sub> nanoparticle sizes has been achieved by hydrolyzing tungsten alkoxide in a reverse microemulsion, forming nanoparticles whose size was controlled between 1.5 nm and 50 nm [47]. WO<sub>3</sub> nanoparticles approximately 1.4 nm in diameter have also been successfully formed in the mesopores of a silica matrix [50].

Recently Pt-WO<sub>3</sub> nanoparticles were synthesized with good control of Pt:W ratio at the nanoparticle level using ethylene glycol as a medium for depositing colloidal Pt and WO<sub>4</sub><sup>2-</sup> precursors [26]. The H<sub>2</sub>PtCl<sub>6</sub> precursor was first reduced in alkaline glycol to a colloidal form and following a decrease in the pH, subsequent deposition of Pt and WO<sub>3</sub> (from WO<sub>4</sub><sup>2-</sup>) was induced. Due to the different and somewhat slow deposition rates of Pt and WO<sub>4</sub><sup>2-</sup>, good particle size control was difficult to achieve. To control both the composition and particle size we

present a new approach to synthesizing nanosized Pt-WO<sub>3</sub> using a microwave-assisted microemulsion methodology. Microwave heating is a good alternative to traditional approaches offering faster, more uniform control of heating and has already been used to successfully synthesize nanosized metal and metal oxide particles including gold [51,52], palladium [53,54], copper oxide [55], tungsten oxide [49], and zinc oxide [56]. In our case, the Pt-WO<sub>3</sub> nanoparticles synthesized in this approach show a narrow size distribution and are well dispersed on a carbon support. We discuss here the details of the synthesis, characterization of the Pt-WO<sub>3</sub> nanoparticles, and the electrocatalytic activities of the nanoparticle system towards methanol oxidation.

## 2. Experimental

### 2.1. Synthesis

All chemicals were of analytical grade and used as received. They include Triton X-100 (t-octylphenoxypolyethoxyethanol) from Sigma Chemical Company, dihydrogen hexachloroplatinate (IV) hydrate (H<sub>2</sub>PtCl<sub>6</sub>·H<sub>2</sub>O) from Chempure Ltd., sodium tungstate (Na<sub>2</sub>WO<sub>4</sub>) from Aldrich Chemical Company, Inc, butan-1-ol and cyclohexane from BDH Chemical Ltd., methanol and sulfuric acid from Aldrich Chemicals. A 10 wt% Pt/Vulcan carbon was supplied by E-TEK Co., and a 5 wt% Nafion solution was used as received from DuPont. All the solutions were prepared using deionized water (18.2 MΩ cm) produced from a Milli-Q ultrapure system of Millipore Ltd., USA.

A typical Pt-WO<sub>3</sub>/carbon catalyst was prepared in two steps as depicted in Fig. 1. Firstly, WO<sub>3</sub> was deposited onto the Vulcan XC-72 carbon by a two-emulsion technique. The two microemulsions had identical fractions of aqueous, surfactant, co-surfactant, and oil phases, but contained different compositions in their aqueous phases, as shown in Table 1. Two 10 ml portions were taken, each from the two microemulsions and mixed together with Vulcan XC-72 carbon by sonicating the solutions for 30 min. The mixed microemulsions were sealed in a HP-500 PTFE reactor and heated in a microwave oven (CEM MARS) at 300 W for 6 min. We observe at 300 W irradiation power, small WO<sub>3</sub> nanoparticles formed only after a minimum of 6 min heating time according to the reaction  $\text{WO}_4^{2-} + 2\text{H}^+ \rightarrow \text{WO}_3 \cdot \text{H}_2\text{O}$ . After cooling to room temperature, the suspension was centrifuged and the solid fraction was washed

**Table 1**  
Compositions of the microemulsion systems used for the synthesis of WO<sub>3</sub> nanoparticles.

	Microemulsion I	Microemulsion II	Volume (ml)
Aqueous phase	20 mM Na <sub>2</sub> WO <sub>4</sub>	0.1 M HCl aq. solution	6
Surfactant	Triton X-100	Triton X-100	12
Co-surfactant	Butan-1-ol	Butan-1-ol	12
Oil phase	Cyclohexane	Cyclohexane	60

**Table 2**  
Compositions of the microemulsion system used for the synthesis of Pt nanoparticles deposited onto WO<sub>3</sub>/C.

	Microemulsion	Volume (ml)
Aqueous phase	10 mM H <sub>2</sub> PtCl <sub>6</sub> aq. solution	6
Surfactant	Triton X-100	12
Co-surfactant	Butan-1-ol	12
Oil phase	Cyclohexane	60

with ethanol and acetone to remove surfactant and any unreacted WO<sub>4</sub><sup>2-</sup>, and then dried at 60 °C in a vacuum oven.

Pt nanoparticles were then deposited on to the carbon supported WO<sub>3</sub> by reducing H<sub>2</sub>PtCl<sub>6</sub> in butan-1-ol. An aqueous solution of H<sub>2</sub>PtCl<sub>6</sub> was used to prepare the microemulsion (Table 2). This Pt containing microemulsion was thoroughly mixed with WO<sub>3</sub>/carbon by sonicating for 30 min. The mixture was sealed in a HP-500 PTFE reactor and heated in the microwave oven at 900 W for 2 min.

We observed that Pt nanoparticles began to form after 1.5 min and that a wider distribution of particle sizes was obtained for lower power and longer exposure times. After heating, the HP-500 PTFE reactor was quickly cooled to room temperature by flowing compressed air over the tube to suppress further nucleation and/or growth of the Pt nanoparticles. The product catalyst was then washed by ethanol and acetone, then dried at 60 °C in a vacuum oven.

As with the recent report on the synthesis of PtWO<sub>3</sub> nanoparticles [26], we used carbon as a support to provide sites for the deposition of the metal from the microemulsions. We propose that the carbon support acts to as a medium for controlling the size of the nanoparticles; for a deposition reaction occurring outside the pores of carbon material, the metal nanoparticles nucleate directly on the carbon and further growth is prevented, while for metal deposition within the pores of carbon, the reaction zones are isolated and small pores limit the growth of the nanoparticles even when surfactant protection is absent. In the earlier reported work [26], a Pt glycol colloidal solution was mixed with a pre-acidified carbon pre-deposited with WO<sub>3</sub> nanoparticles. Since the acidic sites on the carbon are different from the WO<sub>3</sub> sites, pure Pt nanoparticles may be formed away from WO<sub>3</sub>. In the present synthesis, we suggest that the platinum precursor is uniformly impregnated into carbon pores when microwave irradiation is triggered and the Pt nanoparticles preferentially nucleate at the WO<sub>3</sub> sites. As the dielectric constant of carbon is lower than water, the reactions zones can also be confined to individual regions of water within the carbon pores.

**Table 3**  
The composition of the Pt-WO<sub>3</sub>/C catalysts analyzed by EDX.

Pt-WO <sub>3</sub> /C samples	Elements (wt%) <sup>a</sup>		Pt loading on GC electrode (mg cm <sup>-2</sup> )
	Pt	WO <sub>3</sub>	
WO <sub>3</sub> /C	–	12.1%	–
0.5:1	4.73%	11.47%	0.024
1:1	9.36%	10.91%	0.047
2:1	16.57%	10.05%	0.083

<sup>a</sup> Pt and WO<sub>3</sub> loading on Vulcan carbon support were determined by thermal gravimetric analysis (TGA).

Attempts to simultaneously react Pt and W together in a single step microwave exposure did not result in a uniform composition, probably due to the two deposition reactions having different reaction rates. Moreover, reversing the order of preparation by deposition Pt onto carbon first, did not yield a uniform Pt:W ratio. By precipitating WO<sub>3</sub> first, a uniform distribution on the carbon support can be achieved, which can then act as nucleation sites for subsequent uniform deposition of Pt.

## 2.2. Characterization

### 2.2.1. Transmission electron microscopy (TEM)

Transmission electron microscopy analysis of the Pt-WO<sub>3</sub>/C catalyst was performed on a Philips Tecnai G2 20 Scanning TEM operating at 200 kV. High-resolution TEM (HRTEM) images were obtained on a JEOL 2010F TEM. Composition of the nanoparticles was analyzed by an energy-dispersive X-ray (EDX) spectroscope (EDX Microanalysis System, Oxford Instrument) attached to the transmission electron microscope (Philips Tecnai G2 20 Scanning TEM). The samples for analysis were prepared by dispersing nanoparticles in ethanol and drop-casting onto a carbon coated copper grid followed by drying in air at room temperature (22 °C).

### 2.2.2. Thermal gravity analysis (TGA)

The Pt and WO<sub>3</sub> loading on the Vulcan XC-72 carbon support was determined by TGA. Thermal analyses were performed on a PERKIN ELMER TGA-7 Thermogravimetric Analyzer. The samples were held at 50 °C for 10 min then heated to 800 °C at a rate of 10 °C/min under flowing air.

## 2.3. Electrochemical measurements

The working electrodes were prepared by dispersing 5 mg of catalyst in a mixed solution of 0.9 mL ethanol/water (1:1, volume scale) and 0.1 mL Nafion (5 wt%) and sonicating the suspension for 20 min. 20 μL of the suspension was dropped onto on to a glassy carbon electrode (5 mm in diameter) previously polished to mirror-like finish using an alumina suspension. The electrode was then dried at room temperature before use. Table 3 shows the catalyst loading on each of the working electrodes.

All electrochemical tests were performed on a Solatron SI1287 in a three-electrode cell at room temperature (22 °C). A Pt plate and an Hg/Hg<sub>2</sub>SO<sub>4</sub> electrode were used as the counter and the reference electrodes, respectively. A solution of 1 M methanol in 0.5 M H<sub>2</sub>SO<sub>4</sub> was used to study the methanol oxidation activity. The electrolytes were degassed with nitrogen before each electrochemical measurement. Cyclic voltammetry (CV) and chronopotentiometry

(CP) were performed at room temperature (22 °C) to investigate the electrochemical properties of the catalysts.

The electrochemical active surface area (ECSA) of Pt in Pt-WO<sub>3</sub> mixed catalyst system was determined by hydrogen adsorption, CO-stripping method and Cu underpotential deposition/stripping method. In the CO-stripping experiment, the pre-adsorption of CO was achieved by bubbling CO gas into 0.5 M H<sub>2</sub>SO<sub>4</sub> solution, while the potential of working electrode was kept at -0.54 V vs. Hg/Hg<sub>2</sub>SO<sub>4</sub> reference electrode for 20 min. The solution was later purged with N<sub>2</sub> gas for another 30 min to remove the dissolved CO in the solution. The Cu-UPD experiment was conducted according to previous reports [27,57]. In a solution containing 0.002 M CuSO<sub>4</sub>/0.1 M H<sub>2</sub>SO<sub>4</sub>, the working electrode was held at -0.34 V vs. Hg/Hg<sub>2</sub>SO<sub>4</sub> reference electrode for 60 s before the stripping of Cu with a linear scan from -0.34 to 0.46 V vs. Hg/Hg<sub>2</sub>SO<sub>4</sub>.

### 3. Results and discussion

#### 3.1. Characterization

Fig. 2(a) shows a HRTEM micrograph of WO<sub>3</sub> nanoparticles supported on Vulcan XC-72 carbon. The sizes of around 100 WO<sub>3</sub> particles were measured to construct a histogram of the particle size distribution (Fig. 2(b)). These nanoparticles show an average diameter of 1.0 nm. For all batches of the WO<sub>3</sub>/carbon hybrid catalysts prepared by this procedure, a narrow particle size distribution is observed, indicating that the microwave-assisted microemulsion method offers a reproducible route to synthesize WO<sub>3</sub> nanoparticles with a small average size and a narrow particle size distribution. The size of WO<sub>3</sub> nanoparticles can be tuned by varying the composition of microemulsion, the concentration of W and HCl in the precursor solutions, and the microwave irradiation power and heating length. No lattice-fringe images were obtained in the HRTEM analysis and the diffract pattern in the inset of Fig. 2(a) suggests that the WO<sub>3</sub> nanoparticles are amorphous. Longer microwave exposure or higher precursor concentrations leads to the formation of larger WO<sub>3</sub> nanoparticles. Fig. 2(c) shows a TEM micrograph of WO<sub>3</sub> nanoparticles supported on Vulcan XC-72 carbon with an average particle size of 6–10 nm in diameter. This sample was prepared by mixing a 200 mM Na<sub>2</sub>WO<sub>4</sub> microemulsion with a 2 M HCl-containing microemulsion while keeping the other reaction conditions the same as in the sample shown in Fig. 2(a). We observe that high precursor concentration can accelerate the growth of WO<sub>3</sub> nanoparticles. Fig. 2(d) shows size distribution of the nanoparticles.

Batches of Pt-WO<sub>3</sub> nanoparticles with different Pt:W ratios were prepared using the same WO<sub>3</sub>/C starting materials which contain amorphous WO<sub>3</sub> nanoparticles of 1 nm in diameter as shown in Fig. 2(a). The HRTEM images of typical Pt-WO<sub>3</sub> nanoparticles on carbon with 1:1 Pt:W ratio are shown in Fig. 3(a–c). Fig. 3(d) shows that the Pt-WO<sub>3</sub> nanoparticles have an average diameter of 2.5 nm and a narrow size distribution. In HRTEM images of Fig. 3(a–c), crystalline lattice regions are observed. The high intensity lattice spacings of a standard face centered cubic (fcc) Pt crystal are 0.227 nm corresponding to {111} planes and 0.196 nm corresponding to {200} planes. From the HRTEM images and the FFT analyses shown in the insets, only fcc lattices were observed correspond to that of platinum crystals while the rhombic or monoclinic lattices of WO<sub>3</sub> with large spacings were not observed. This, however, cannot rule out the presence of WO<sub>3</sub> domains adjacent to Pt nanoparticles. The small WO<sub>3</sub> nanoparticles, if present, as in Fig. 2(a) would be amorphous. In the HRTEM images of PtWO<sub>3</sub> samples, we cannot not observe individual small amorphous nanoparticles as in Fig. 2(a) while the corresponding EDX analysis (as shown in Fig. 5) of the same TEM sample indicates the presence of tungsten. The WO<sub>3</sub>

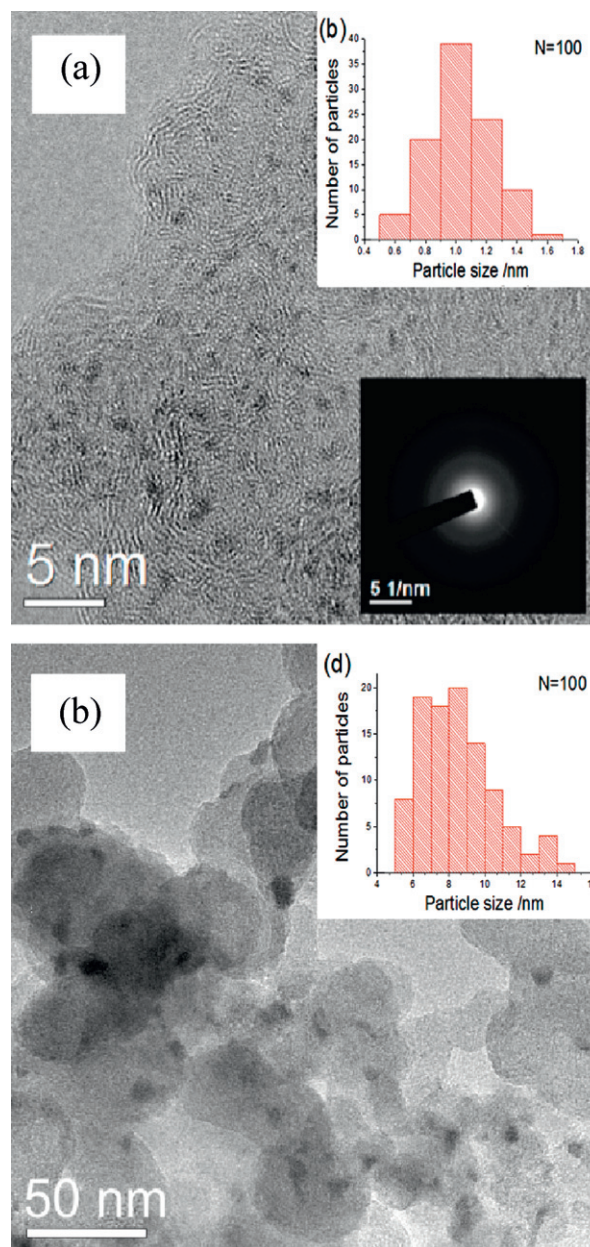


**Fig. 2.** (a) HRTEM image of the as-synthesized WO<sub>3</sub> nanoparticles supported on VC X-72 carbon. (b) Histogram of particle size distribution for 100 WO<sub>3</sub> particles. (c) TEM images of the WO<sub>3</sub> nanoparticles supported on VC X-72 carbon synthesized with high precursor concentration. (d) Histogram of particle size distribution for 100 WO<sub>3</sub> particles.

domains are therefore most likely to be covered or overlapped with Pt fcc nanoparticles. The lattice spacings in Fig. 3(a), (b), and (c) are 0.224, 0.223, 0.224, 0.197, 0.195, 0.198 nm, which are slightly different from the standard values of fcc Pt. It is possible that the lattice spacing is affected by the presence of W and O atoms. Many nanoparticles show clear flat surfaces and edges with definite angles, which is uncommon for Pt nanoparticles as small as 2.5 nm. This suggests some influence of WO<sub>3</sub> domains on the lattice structure of adjacent Pt nanocrystals. It is unclear whether and how the interfaces of adjacent domains of Pt and WO<sub>3</sub> enhance the electrocatalytic activity for methanol oxidation.

From electrochemical surface area measurements, as discussed in later section and shown in Table 4, the Pt surface area increase with the presence of WO<sub>3</sub>, as compared to the case of pure Pt

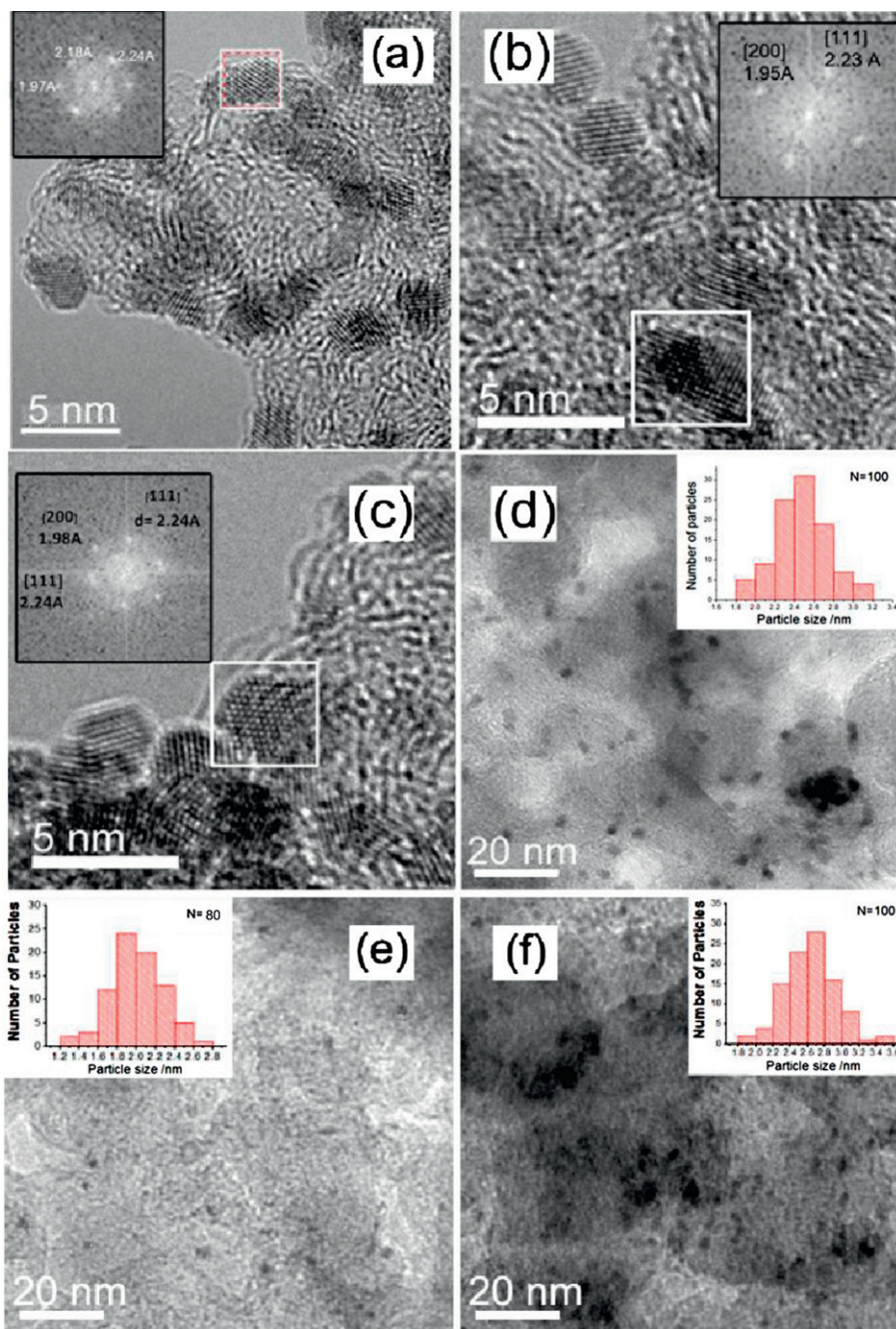


**Fig. 3.** (a)–(c) HRTEM images of Pt-WO<sub>3</sub> nanoparticles supported on VC X-72 carbon with 1:1 Pt:W ratio with inserted FFT analysis of the region marked by the white rectangular. (d)–(f) TEM images with inserted histograms of particle size distribution for Pt-WO<sub>3</sub> nanoparticles (d) Pt:W = 1:1, (e) Pt:W = 0.5:1 and (f) Pt:W = 2:1.

**Table 4**  
The electrochemical active surface area (ECSA) of Pt sites in Pt-WO<sub>3</sub>/C catalysts determined by H-adsorption, CO-stripping, and Cu-UPD method. (\*Note: Pt surface area is calculated based on the average Pt particle sizes estimated by TEM, assuming that all Pt particles are spherical and with the same diameter. The estimated average particle sizes for Pt-WO<sub>3</sub>/C catalysts with Pt:W ratio = 0.5:1, 1:1, and 2:1 are 1.8, 2.5, and 2.7 nm, respectively.)

Pt:W ratio in samples	ECSA of Pt (m <sup>2</sup> g <sup>-1</sup> )			Pt surface area estimated from TEM* (m <sup>2</sup> g <sup>-1</sup> )
	By H adsorption	By CO-stripping	By Cu-UPD	
0.5:1	163	149	129	155
1:1	174	133	108	112
2:1	116	96	97	104
1:0 (E-TEK Pt/C)	89	94	86	93

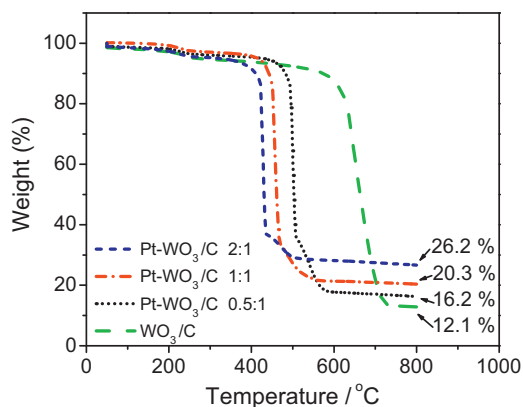


**Fig. 4.** Thermal gravimetric analysis (TGA) of as-synthesized  $\text{WO}_3/\text{C}$  and  $\text{Pt-WO}_3/\text{C}$  electrocatalysts with different compositions.

nanoparticles. This also suggests deposition of platinum onto the small amorphous  $\text{WO}_3$  nanoparticles.

### 3.2. Control of Pt:W ratio

The  $\text{WO}_3$  and Pt weight percentage of the  $\text{WO}_3/\text{C}$  and  $\text{Pt-WO}_3/\text{C}$  catalysts were summarized in Table 3. They were determined by TGA results in Fig. 4 and Pt:W ratio from EDX analyses. It is known that ionic surfactants are difficult to remove from the surface of nanoparticles. In our synthesis, non-ionic surfactant Triton X-100 was used. TGA analysis showed that Triton X-100 was removed successfully after washing by ethanol and acetone for 4–6 times. The chemical compositions of the as-synthesized catalysts were confirmed by EDX measurements. Different regions with analytical areas of approximately  $100 \text{ nm}^2$  were randomly selected and analyzed. Fig. 5 shows a typical EDX spectrum of the  $\text{Pt-WO}_3/\text{C}$  catalysts with a 1:1 Pt:W ratio. In different analytical regions the Pt:W ratio was found to be consistently 1:1. The EDX spectrum shows, in addition to Pt and W, C and O. The loading of Pt and W cannot be determined by EDX analysis as a carbon TEM grid was used. The absence of a chlorine and sodium peaks indicates that the chlorine and sodium ions were completely removed in the washing steps. Since the same starting  $\text{WO}_3/\text{C}$  materials was used to prepare various electrocatalyst of different Pt:W ratios, the Pt:W ratios in the synthesized products can also be calculated from the TGA results of different samples. The results of TGA are consistent with those analyzed by EDX.

Fig. 6 compares the Pt:W ratio in the each of the synthesized catalyst with the initial Pt:W ratio used in the precursors. The Pt:W

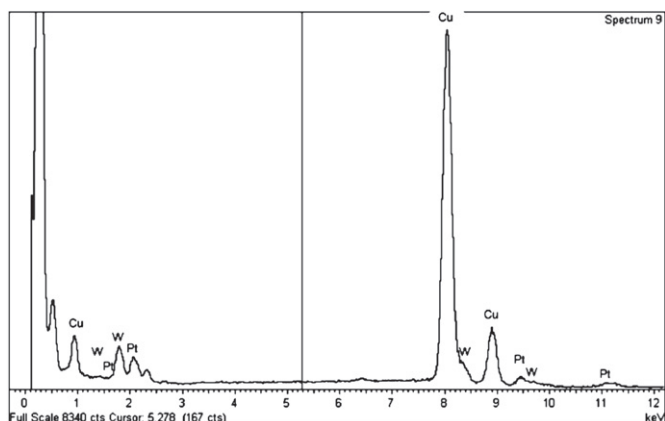


**Fig. 5.** EDX spectrum of the  $\text{Pt-WO}_3/\text{C}$  catalyst (Pt:W = 1:1).

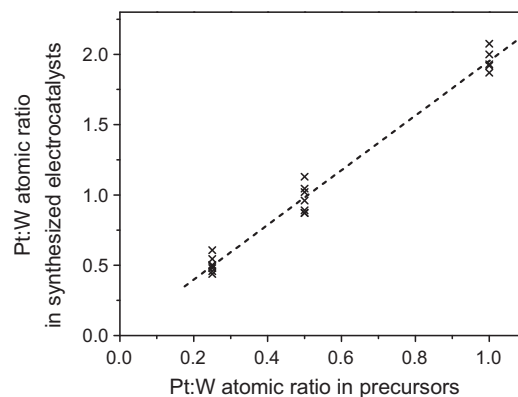


**Fig. 6.** Correlation of Pt:W atomic ratio in the synthesized  $\text{Pt-WO}_3/\text{C}$  catalysts to Pt:W atomic ratio in precursors. (Note: Pt:W atomic ratios in the synthesized  $\text{Pt-WO}_3/\text{C}$  catalysts are obtained from EDX analysis, as described in Section 2.)

ratio across the different areas analyzed are in close agreement. A higher W content in the initial precursor indicates that the precipitation of tungsten oxide or the adsorption onto carbon support may not be completed in the first  $\text{WO}_3$  synthesis step. However, this incomplete reaction, does not affect the control of the Pt:W ratio in the final product and we are able to control the Pt:W ratio simply by changing the amount of Pt containing microemulsion added in the second step while using the same reaction conditions in the first  $\text{WO}_3$  precipitation step.

### 3.3. Measurement of Pt active surface area

The measurement of electrochemical active surface area of the catalysts is important to evaluate electrocatalytic activity based on accessible surface. We have separately evaluated ECSA based on three methods, viz. electrosorption of hydrogen, CO stripping and Cu-UPD stripping.

#### 3.3.1. ECSA by hydrogen adsorption

The active surface area of a Pt catalyst is usually determined by hydrogen adsorption/desorption assuming that a monolayer of adsorbed H formed on the surface Pt sites [58,59]. The charge associated with the  $\text{H}^+$  adsorption–desorption reaction on Pt sites is  $210 \mu\text{C cm}^{-2}$ , related to the number of platinum atoms exposed [59].



For  $\text{Pt-WO}_3/\text{C}$  catalyst, the hydrogen desorption method (in the potential region 0–0.3 V vs. RHE) faces uncertainty because of the interaction between  $\text{WO}_3$  and protons forming tungsten bronzes in the potential region of 0–0.55 V vs. RHE [29,36,37,60–62]. Fig. 7(a) shows the cyclic voltammograms in sulfuric acid medium of 12.8 wt%  $\text{WO}_3$  on Vulcan carbon in contrast to blank Vulcan XC-72 carbon. It can be observed that the interaction of protons and  $\text{WO}_3$  is taking place forming tungsten bronze in the potential region of –0.64 V to –0.2 V vs.  $\text{Hg}/\text{Hg}_2\text{SO}_4$ . This overlaps with  $\text{H}_2$  adsorption–desorption region on Pt. A possible method to evaluate the electrochemical surface area due to Pt alone is to subtract the H adsorption peaks due to pure  $\text{WO}_3$  in Fig. 7(a). The ECSA thus determined are tabulated in Table 4. This decoupling of H sorption due to  $\text{WO}_3$ , however, is problematic since  $\text{H}^+$  sorption on  $\text{WO}_3$  can be catalyzed by the presence of Pt, as pointed out by Kulesza et al. [64] and Tseung et al. [29,32,36,37]. The H-sorption determined ECSA values in Table 4 are therefore systematically higher than corresponding values determined by CO-stripping and Cu-UPD methods which are described below.

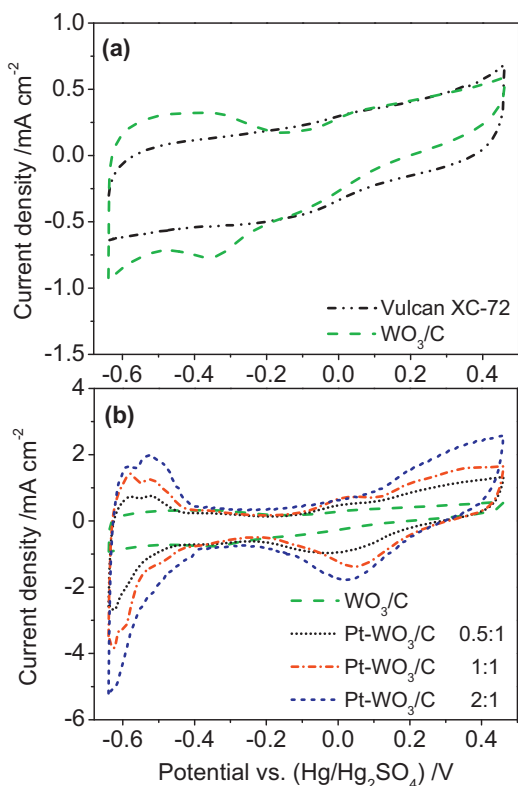


**Fig. 7.** Cyclic voltammograms of (a)  $\text{WO}_3/\text{C}$  and (b)  $\text{Pt-WO}_3/\text{C}$  electrocatalysts in  $0.5\text{ M H}_2\text{SO}_4$  at a scan rate of  $20\text{ mV s}^{-1}$ . The current scale is normalized by the geometrical electrode area ( $0.196\text{ cm}^2$ ).

### 3.3.2. ECSA by CO stripping

CO-stripping voltammetry is an alternative method for measuring the electrochemical surface area of Pt [61,62,24,63]. It is generally agreed that CO adsorbs on Pt in a 1:1 linearly bonded fashion, assuming the charge associated in the CO monolayer adsorption on Pt site is  $420\text{ }\mu\text{C cm}^{-2}$ .

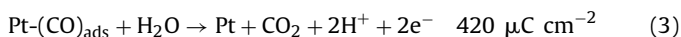
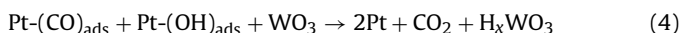


Fig. 8 shows the CV curves for CO stripping on  $\text{WO}_3/\text{C}$ ,  $\text{Pt}/\text{C}$  and  $\text{Pt-WO}_3/\text{C}$  composite electrodes with various Pt:W ratio. The oxidation peak for CO on  $\text{Pt-WO}_3/\text{C}$  (1:1) electrode is 46 mV compared to 96 mV (vs.  $\text{Hg}/\text{Hg}_2\text{SO}_4$ ) for  $\text{Pt}/\text{C}$  from E-TEK. For the  $\text{Pt-WO}_3/\text{C}$  (0.5:1) and (2:1) electrodes, the CO oxidation peaks were also negatively shifted, but to a smaller extent of about 30 mV. These results suggest that the  $\text{WO}_3$  nanoparticles promote CO oxidation on Pt [33,39,40]. The mechanism can be described in the following reaction:



Jayaraman et al. [27] speculated that CO can also oxidize on the surface of  $\text{WO}_3$ . They found that tungsten changes oxidation states between +6 and +5, providing the oxygen species required for the removal of CO [27]. From Fig. 8(a), no CO stripping peak is observed in pure  $\text{WO}_3$  sample. This may be due to little CO adsorption on  $\text{WO}_3$  during the CO pretreatment step, rather than inability of CO oxidation on  $\text{WO}_3$  surface. The absence of CO stripping current in  $\text{WO}_3$  enables a distinct evaluation of Pt surface area available to CO sorption. The complication of  $\text{WO}_3$  on amount of CO stripping from Pt still exists, however, since CO adsorption at  $E=0.1\text{ V}$  vs. RHE on  $\text{Pt-WO}_3$  nanoparticles yields production of  $\text{CO}_2$  at  $E=0.1\text{ V}$  vs. RHE, as nicely demonstrated by Micoud et al. with FTIR [39]. The method of stripping under-potential deposited copper is therefore applied as described below.

### 3.3.3. ECSA by Cu-UPD stripping

Using CO-stripping voltammetry to determine the electrochemical surface area of Pt has the ambiguity in the adsorption mode of CO on Pt site in the presence of alloyed metal/metal oxide, whether CO is linearly bonded or bridge-bonded [57]. Green and Kucernak reported the determination Pt and Ru surface areas in Pt-Ru alloys by the Cu-UPD method [57]. In this method, a monolayer of Cu is underpotential deposited, and from the stripping voltammograms, the surface area of Pt and Ru can be estimated separately. Jayaraman and McFarland later applied this method on  $\text{Pt-WO}_3$  mixed catalyst system to estimate the Pt surface area [27]. The copper stripping reaction is a two-electron-transfer reaction in the potential region of  $0.3\text{--}0.8\text{ V}$  vs. RHE, and the charge associated with this reaction is  $420\text{ }\mu\text{C cm}^{-2}$  [27,54].



The Cu-UPD stripping method proves to be a viable method for Pt surface area determination in  $\text{Pt-WO}_3$  catalysts [27]. Fig. 9 shows the Cu underpotential deposition/stripping experiments on  $\text{WO}_3/\text{C}$ ,  $\text{Pt}/\text{C}$  (E-TEK) and  $\text{Pt-WO}_3/\text{C}$  composite electrodes. In Fig. 9(a), the curve 1 is the cyclic voltammogram of the  $\text{WO}_3/\text{C}$  electrode in  $0.1\text{ M H}_2\text{SO}_4$ . Curves 2 and 3 are the cyclic voltammograms of the  $\text{WO}_3/\text{C}$  electrode in  $0.002\text{ M CuSO}_4/0.1\text{ M H}_2\text{SO}_4$  with different potential scan windows. It can be observed that curve 3 overlapped with curve 1, indicating no underpotential deposition or stripping of Cu occurs on  $\text{WO}_3/\text{C}$  electrode in the potential region of  $-0.34\text{ V}$  to  $0.46\text{ V}$  vs.  $\text{Hg}/\text{Hg}_2\text{SO}_4$ . Notably, Fig. 9(b) shows the Cu-UPD on  $\text{Pt}/\text{C}$  electrode. The anodic peaks indicate that underpotential deposition of Cu has occurred on Pt during the initial holding potential at  $-0.34\text{ V}$  vs.  $\text{Hg}/\text{Hg}_2\text{SO}_4$ . These results show that Cu-UPD method can be used to determine the Pt surface area in  $\text{Pt-WO}_3$  mixed catalyst system.

The electrochemical surface areas of Pt in  $\text{Pt-WO}_3/\text{C}$  catalysts determined by hydrogen adsorption, CO-stripping, and Cu-UPD stripping methods are summarized in Table 4. ECSA was calculated by  $Q/[\text{Pt}Q^0]$ , where  $Q$  is the charge involved in the adsorption and desorption reaction occurred on the surface of Pt while  $[\text{Pt}]$  represented the Pt mass loading on the electrode.  $Q^0$  is the monolayer adsorption charge. It is notable that the surface areas of Pt estimated by hydrogen adsorption method were larger than by using CO-stripping and Cu-UPD method, possibly due to the involvement of  $\text{H}_x\text{WO}_3$  in the sensitivity to potential limits of adsorption.

### 3.3.4. Estimation of ECSA from TEM images

Pt surface area can also be estimated from TEM images shown in Fig. 3. The nanoparticles within each sample are assumed to be pure Pt, perfect spheres, and uniform in size as determined by the peak of the particle size distributions of Fig. 3(d), (e) and (f). The surface areas thus determined are listed in the last column of Table 4. For a 3 nm diameter pure Pt nanoparticle, the estimated Pt surface area is  $93\text{ m}^2\text{ g}^{-1}\text{ Pt}$ . The ECSA of the E-TEK  $\text{Pt}/\text{C}$  sample measured electrochemically has values between  $89$  and  $94\text{ m}^2\text{ g}^{-1}\text{ Pt}$  which is close to this TEM estimation. In addition to the fully exposed perfect spheres of uniform size, other uncertainties exist in this approach. It is not clear whether only Pt regions are visible in TEM images of Fig. 3, and whether Pt forms its own particle on top of  $\text{WO}_3$  domain; or  $\text{WO}_3$  are integrated into  $\text{PtWO}_3$  nanoparticles. There is absence of any characteristic feature of  $\text{WO}_3$  lattice in the TEM images and the corresponding FFT patterns in Fig. 3. The  $\text{WO}_3$  however, may be present in amorphous form as in Fig. 2(a). The TEM particle size can be larger than the size of Pt regions and the corresponding calculated surface area will be an underestimation since Pt can be more dispersed. On the other hand, the assumption of a fully exposed sphere is an over-estimation since a good part of the particle can be embedded in the support. The Pt surface area estimated by TEM which is a non-electrochemical measurement, will not be the same

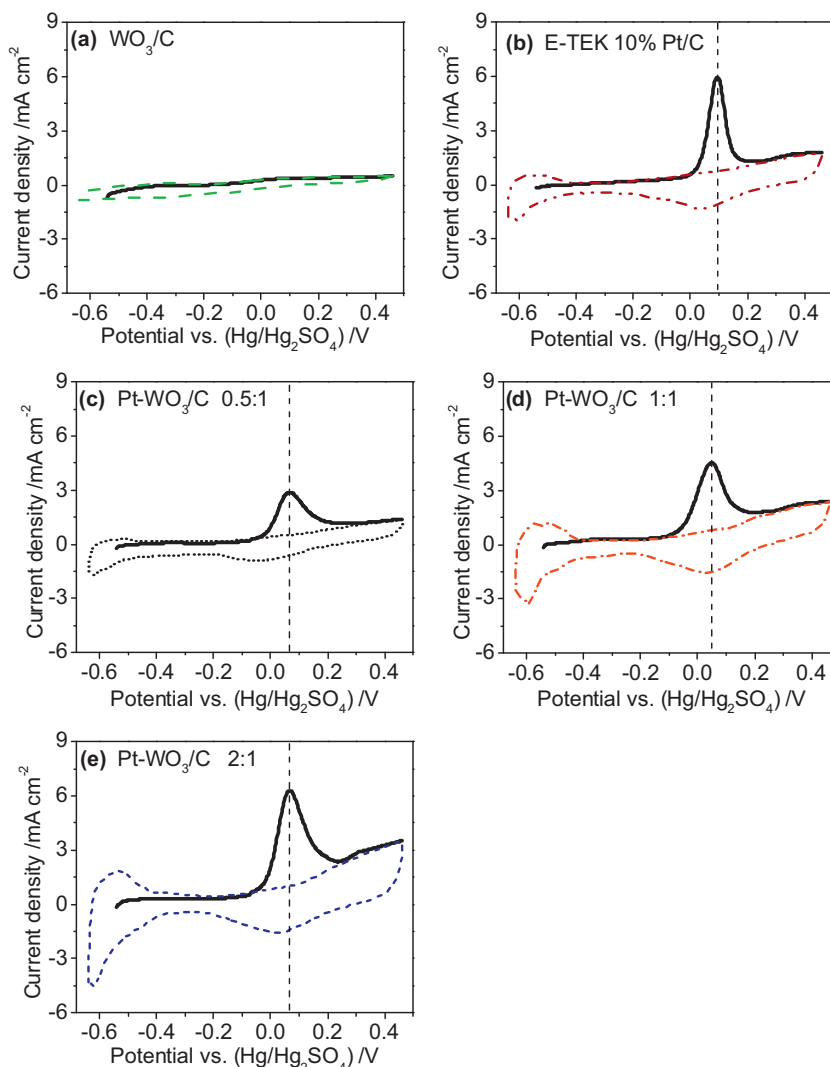


**Fig. 8.**  $\text{CO}_{\text{ads}}$  stripping voltammograms recorded at  $20 \text{ mV s}^{-1}$  in  $0.5 \text{ M H}_2\text{SO}_4$  for (a)  $\text{WO}_3/\text{C}$  and (b) 10 wt% Pt/C from E-TEK, and (c)–Pt- $\text{WO}_3/\text{C}$  electrocatalysts with different Pt:W ratios. Solid black lines show the first scan (i.e., the CO stripping peak) while the dotted lines show the second scan (i.e., the background CV curves of the electrode in  $0.5 \text{ M H}_2\text{SO}_4$ ). The current scale is normalized by the geometrical electrode area ( $0.196 \text{ cm}^2$ ).

as ECSA area, but serving as a reference. The Cu-UPD values are taken as more reliable representations of ECSA. The deviations in ECSA values determined by different methods are small in the case of pure Pt nanoparticles and increase with W content.

#### 3.4. Methanol oxidation measurements

Performance of the electrocatalysts was evaluated for oxidation of methanol by performing cyclic voltammetry and chronopotentiometry experiments. The electrochemical behavior of Pt- $\text{WO}_3/\text{C}$  composite catalysts with three different Pt:W ratios (0.5:1, 1:1, and 2:1) were compared to a commercial E-TEK 10 wt% Pt/C catalyst. Fig. 10 shows the cyclic voltammograms of Pt- $\text{WO}_3/\text{C}$  and E-TEK Pt/C composite catalysts for methanol oxidation in  $1.0 \text{ M CH}_3\text{OH} + 0.5 \text{ M H}_2\text{SO}_4$  electrolyte and the current reported was normalized by Pt mass and ECSA of Pt estimated by Cu-UPD method. Each voltammogram was recorded after 10 initial cycles. Some characteristic parameters of the CVs are summarized in Table 5, in which  $E_{1/2}$  is the anodic half-peak potential,  $j_{\text{mass}}$  and  $j_{\text{ECSA}}$  represent activities based on Pt-mass and Pt-surface-area, respectively. No current peak was observed in the CV curve for  $\text{WO}_3/\text{C}$  indicating the absence of catalytic activity for methanol oxidation. For

the Pt- $\text{WO}_3$  catalysts, oxidation of methanol starts from  $-0.1 \text{ V}$  vs.  $\text{Hg}/\text{Hg}_2\text{SO}_4$  and reaches a peak at about  $0.2 \text{ V}$  vs.  $\text{Hg}/\text{Hg}_2\text{SO}_4$ . The highest activity is observed in the Pt- $\text{WO}_3$  electrocatalyst with 1:1 Pt:W atomic ratio, whether based on Pt-mass or Pt ECSA. The anodic peak current density of 1:1 Pt- $\text{WO}_3/\text{C}$  was  $271 \text{ mA mg}^{-1} \text{ Pt}$  which is 1.4 times that of E-TEK Pt/C catalyst.

A constant current experiment was conducted to evaluate steady-state methanol oxidation by the best performing 1:1 Pt:W ratio catalyst. The chronopotentiogram in Fig. 11 was performed at a  $110 \text{ mA mg}^{-1} \text{ Pt}$  and a very steady oxidizing potential can be achieved for over 6 min.

#### 3.5. Pt:W ratio and role of $\text{WO}_3$ in Pt activity

For the composite Pt- $\text{WO}_3$  catalyst synthesized by the microwave-assisted microemulsion method, the presence of  $\text{WO}_3$  can physically and chemically affects the catalytic performance of Pt nanoparticles. As shown in Table 4, the ECSA of various Pt- $\text{WO}_3$ , determined by different methods, all show higher areas with higher W content. As discussed earlier, the ECSA determined by Cu-UPD stripping is more reliable and least chemically affected. The Cu-UPD value is  $129 \text{ m}^2 \text{ g}^{-1} \text{ Pt}$  for the Pt:W=0.5:1 sample,

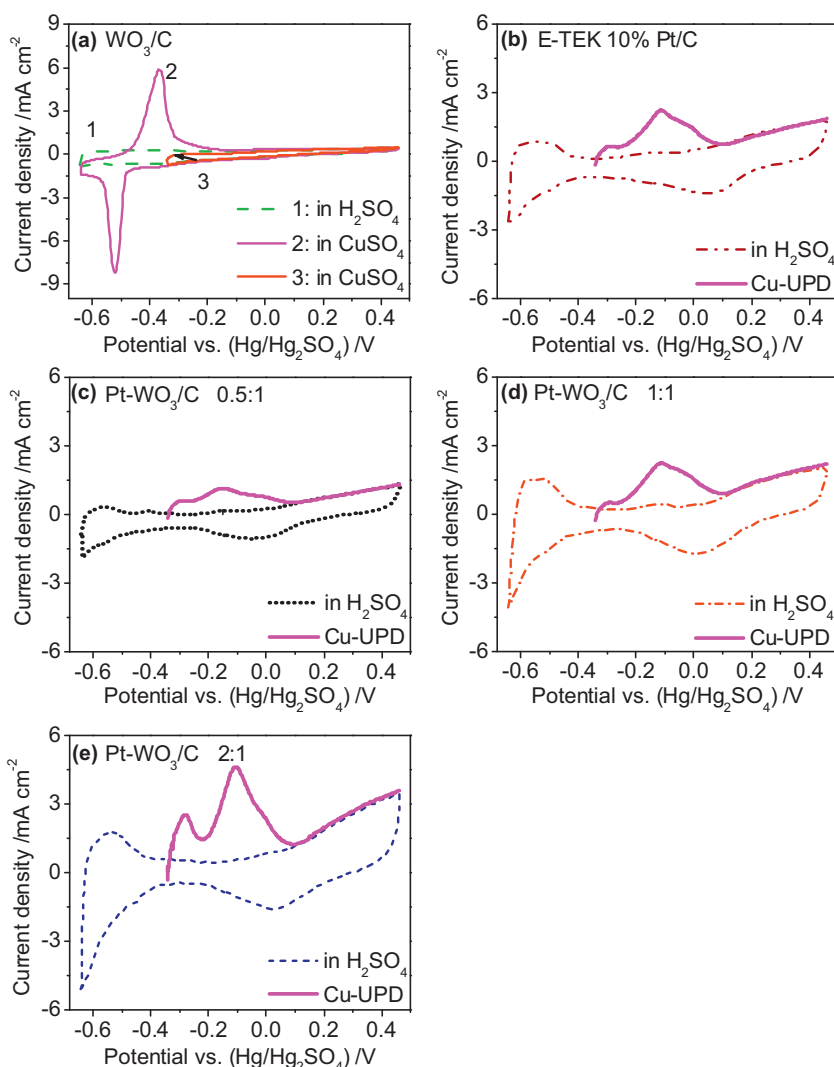


**Fig. 9.** (a) Cu deposition experiments on  $\text{WO}_3/\text{C}$  electrode: (1) Cyclic voltammograms of  $\text{WO}_3/\text{C}$  in 0.1 M  $\text{H}_2\text{SO}_4$  at a scan rate of  $20 \text{ mV s}^{-1}$  and (2) (3) Cyclic voltammograms of  $\text{WO}_3/\text{C}$  in 0.002 M  $\text{CuSO}_4/0.1 \text{ M H}_2\text{SO}_4$  at a scan rate of  $20 \text{ mV s}^{-1}$  with different potential scan windows. (b)–(e) Cu-UPD experiments on Pt- $\text{WO}_3/\text{C}$  composite electrodes with different Pt:W ratios. Cu-stripping voltammogram (Solid line) was recorded in 0.002 M  $\text{CuSO}_4/0.1 \text{ M H}_2\text{SO}_4$  at a scan rate of  $20 \text{ mV s}^{-1}$  with potential held at  $-0.34 \text{ V}$  vs.  $\text{Hg}/\text{Hg}_2\text{SO}_4$  for 60 s before the start of stripping to  $0.46 \text{ V}$  vs.  $\text{Hg}/\text{Hg}_2\text{SO}_4$ . The dotted lines show the control experiments of CV in 0.1 M  $\text{H}_2\text{SO}_4$  with a larger potential window showing no stripping current. The current scale is normalized by the geometrical electrode area ( $0.196 \text{ cm}^2$ ).

decreased to  $97 \text{ m}^2 \text{ g}^{-1}$  Pt for the Pt:W=2:1 sample and a value of  $86 \text{ m}^2 \text{ g}^{-1}$  Pt in for pure Pt on carbon. This enhancement of the Pt- $\text{WO}_3/\text{C}$  catalysts is due to better dispersion of Pt with smaller particle size (3.1 nm of pure Pt particles vs. 1.8 of 0.5:1 Pt:W catalyst as estimated by TEM). The chemical enhancement effect is evident since there is enhanced H sorption on  $\text{WO}_3$ , negative shifts in CO oxidation, and the ECSA values determined by other methods are higher than the Cu-UPD value of  $129 \text{ m}^2 \text{ g}^{-1}$  Pt in the case of Pt:W=0.5:1 while more or less in agreement for pure Pt nanoparticles.

**Table 5**  
Electrocatalytical performance data from cyclic voltammograms (Fig. 10) of electrodes with different Pt:W ratios. \*Note that  $E_{1/2}$  is the anodic half-peak potential,  $j_{\text{mass}}$  is the specific current density normalized by Pt mass,  $j_{\text{ECSA}}$  is the specific current density normalized by the electrochemical active surface area (ECSA) of Pt obtained by Cu-UPD method.

Pt:W ratio in samples	Forward anodic peak		
	$E_{1/2}$ vs. ( $\text{Hg}/\text{Hg}_2\text{SO}_4$ ) (V)	$j_{\text{mass}}$ ( $\text{mA mg}^{-1}$ )	$j_{\text{ECSA}}$ ( $\text{mA cm}^{-2}\text{-Pt}$ )
0.5:1	0.017	256	0.198
1:1	0.013	271	0.251
2:1	0.047	206	0.213
E-TEK 10% Pt	0.028	187	0.217

After normalization to ECSA of Pt, the specific activities of the Pt- $\text{WO}_3$  samples are similar, as shown in the anodic forward scans of Fig. 10(b). The peak current densities per Pt area  $j_{\text{ECSA}}$  are compared in Table 5. The case of Pt:W=1:1 still gives the best specific activity compared to 0.5:1 and 2:1, indicating an optimum ratio of Pt to  $\text{WO}_3$ . The onset potentials were similar among the Pt- $\text{WO}_3$  samples, but lowest for Pt:W=0.5:1 with value of  $-0.17 \text{ V}$  (vs.  $\text{Hg}/\text{Hg}_2\text{SO}_4$ ). This compares well to the onset potential of Pt/C (E-TEK) at  $-0.1 \text{ V}$  (vs.  $\text{Hg}/\text{Hg}_2\text{SO}_4$ ). The onset potentials of the sample catalysts can be ranked in the order of 0.5:1 < 1:1 < 2:1 < Pt/C. These

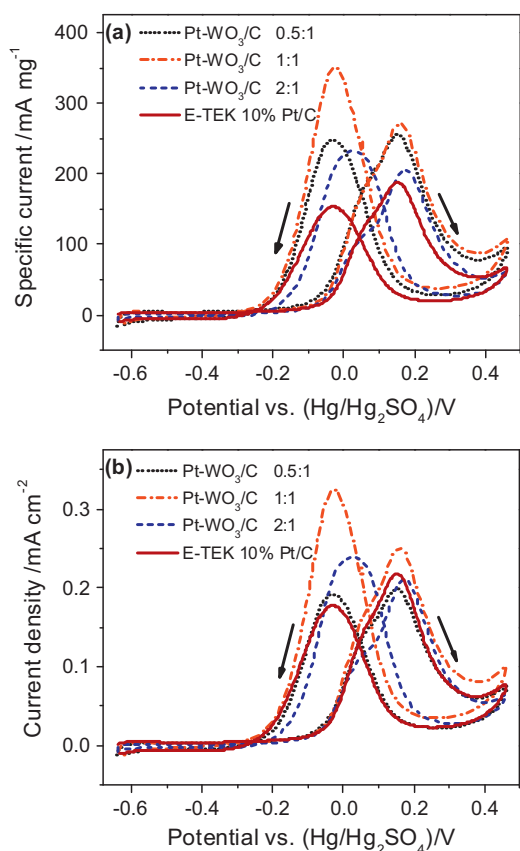


**Fig. 10.** Cyclic voltammograms of the Pt-WO<sub>3</sub>/C electrocatalysts with different Pt:W ratios in 1.0 M CH<sub>3</sub>OH + 0.5 M H<sub>2</sub>SO<sub>4</sub> at room temperature. Scan rate is 20 mV s<sup>-1</sup>. Current scale is normalized by the Pt-mass (a) and by the Pt surface area estimated from Cu-UPD stripping experiments (b).

negative shifts suggest some chemical effects of WO<sub>3</sub> in promoting methanol oxidation on Pt.

Methanol oxidation reaction is a six-electron-transfer reaction. It is generally thought that methanol oxidation over Pt occurs when methanol molecules (CH<sub>3</sub>OH) adsorbed on Pt and subsequently dissociate to form a Pt-(CHO)<sub>ads</sub> intermediate. This intermediate further reacts with Pt-(OH)<sub>ads</sub> to give CO<sub>2</sub> and H<sup>+</sup>. The reaction mechanism is proposed by several researchers in literatures [36,37,64], as shown in the following chemical reactions:

Normal Pt catalysis mechanisms:

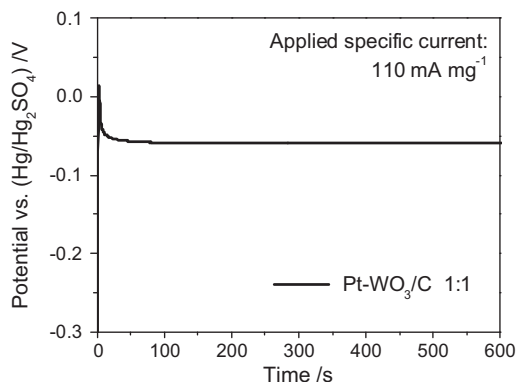
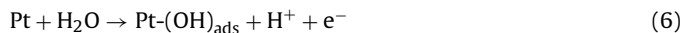
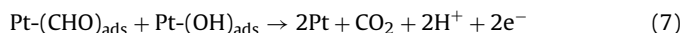


**Fig. 11.** Chronopotentiogram of methanol oxidation on Pt-WO<sub>3</sub>/C (1:1 Pt:W ratio) at 110 mA mg<sup>-1</sup> Pt. Electrolyte is 0.5 M H<sub>2</sub>SO<sub>4</sub> containing 1.0 M CH<sub>3</sub>OH.



Chemically, the abundant interfaces between Pt and WO<sub>3</sub> nanoparticles enhance the hydrogen spillover effects. Hydrogen spill over onto the surface of WO<sub>3</sub> and form hydrogen tungsten bronze (H<sub>x</sub>WO<sub>3</sub>), free the active Pt sites for further chemisorption of methanol molecules and make the dehydrogenation of methanol molecules adsorbed on Pt sites more effective [29,30,41]. In addition, WO<sub>3</sub> also takes part in removal of CO. The oxophilic nature of the oxide helps in removing the adsorbed intermediates during the methanol oxidation [30]. Since CO removal is the rate-limiting step of the methanol oxidation [27], this intrinsic improvement in CO oxidation will lead to an overall improved performance of Pt-WO<sub>3</sub> catalysts for methanol oxidation.

#### 4. Conclusions

Nanoparticle size and composition control of a Pt-WO<sub>3</sub>/C catalyst was achieved through the reaction of a water-oil microemulsion using microwave irradiation in a two-step process: WO<sub>3</sub> nanoparticles were first deposited on Vulcan XC-72 carbon by mixing of two microemulsion systems containing HCl and WO<sub>4</sub><sup>2-</sup>, to yield WO<sub>3</sub>/C, followed by the subsequent addition of Pt by microwave irradiation of a Pt-containing microemulsion. TEM images showed homogenous distribution of WO<sub>3</sub> nanoparticles on the carbon support with an average size of 1 nm. Under microwave irradiation, butan-1-ol, the co-surfactant of the microemulsion system, played a role of reducing agent and successfully reduced hexachloroplatinic acid to Pt nanoparticles. The PtWO<sub>3</sub> nanoparticles produced in this step had an average size of 2.5 nm. EDX analysis at different locations confirmed the Pt:W ratio of the as-synthesized Pt-WO<sub>3</sub>/C catalyst was homogeneous. The electrochemical experiments showed that these Pt-WO<sub>3</sub>/C nanoparticles have high catalytic activity toward methanol oxidation at room temperature (22 °C). Hydrogen adsorption, CO-stripping and Cu-UPD stripping methods were used to estimate electrochemical active surface area of Pt in the Pt-WO<sub>3</sub>/C catalysts, in which Cu-UPD method is relative more reliable due to the involvement of WO<sub>3</sub> component. Pt-WO<sub>3</sub>/C electrocatalysts with large WO<sub>3</sub> component present higher Pt surface area, suggesting that WO<sub>3</sub> nanoparticles supported on carbon greatly improve the distribution of Pt nanoparticles. CO-stripping experiments show an intrinsic enhancement of CO oxidation for Pt-WO<sub>3</sub>/C catalysts by comparing the onset potential of CO stripping [27,39,40]. The methanol oxidation measurement shows that a 1:1 Pt:W ratio catalyst exhibits the highest Pt-mass current density of 271 mA mg<sup>-1</sup>, 1.4 times higher than that of commercial E-TEK catalyst. However, the specific catalytic activities based on Pt-surface-area appear less difference. Therefore, the enhancement in catalytic activity mainly comes from two parts: the physical modification of Pt from WO<sub>3</sub> nanoparticles, such as surface area, and the chemical effects, such as improved performance on hydrogen spillover and CO oxidation.

#### Acknowledgments

This work was supported by the Hong Kong Research Grants Council (GRF HKU 700209P), and the HKU Development Fund for the Initiative of Clean Energy and Environment. We thank the University of Hong Kong Electron Microscope Unit for the use of TEM and EDX facilities. The HRTEM work was performed in MCPF of HKUST.

#### References

- [1] L. Carrette, K.A. Friedrich, U. Stimming, *ChemPhysChem* 1 (2000) 162.
- [2] M. Winter, R.J. Brodd, *Chemical Reviews* 104 (2004) 4245.
- [3] N. Kizhakevariam, E.M. Stuve, *Surface Science* 286 (1993) 246.

- [4] S. Mukerjee, R.C. Urian, *Electrochimica Acta* 47 (2002) 3219.
- [5] L.G.S. Pereira, V.A. Paganin, E.A. Ticianelli, *Electrochimica Acta* 54 (2009) 1992.
- [6] C. Bock, C. Paquet, M. Couillard, G.A. Botton, B.R. MacDougall, *Journal of American Chemical Society* 126 (2004) 8028.
- [7] W.M. Chen, G.Q. Sun, Z.X. Liang, Q. Mao, H.Q. Li, G.X. Wang, Q. Xin, H. Chang, C.H. Pak, D.Y. Seung, *Journal of Power Sources* 160 (2006) 933.
- [8] N.P. Lebedeva, G.J.M. Janssen, *Electrochimica Acta* 21 (2005) 29.
- [9] L. Li, B.Q. Xu, *Acta Physico-Chimica Sinica* 21 (2005) 1132.
- [10] X. Li, G. Chen, J. Xie, L.J. Zhang, D.G. Xia, Z.Y. Wu, *Journal of Electrochemical Society* 157 (2010) B580–B584.
- [11] X.Z. Cui, J.L. Shi, L.X. Zhang, M.L. Ruan, J.H. Gao, *Carbon* 47 (2009) 186.
- [12] C.W. Xu, Y.Z. Su, L.L. Tan, Z.L. Liu, J.H. Zhang, S.A. Chen, S.P. Jiang, *Electrochimica Acta* 54 (2009) 6322.
- [13] K.R. Lee, M.K. Jeon, S.I. Woo, *Applied Catalysis B–Environmental* 91 (2009) 428.
- [14] L.X. Yang, R.G. Allen, K. Scott, P. Christenson, S. Roy, *Journal of Power Sources* 137 (2004) 257.
- [15] T. Kawaguchi, Y. Rachi, W. Sugimoto, Y. Murakami, Y. Takasu, *Journal of Applied Electrochemistry* 36 (2006) 1117.
- [16] F. Peng, C.M. Zhou, H.J. Wang, H. Yu, J.H. Liang, J.A. Yang, *Catalysis Communications* 10 (2009) 533.
- [17] K. Drew, G. Girishkumar, K. Vinodgopal, P.V. Kamat, *Journal of Physical Chemistry B* 109 (2005) 11851.
- [18] K.W. Park, S.B. Han, J.M. Lee, *Electrochemistry Communications* 9 (2007) 1578.
- [19] C.L. Campos, C. Roldan, M. Aponte, Y. Ishikawa, C.R. Cabrera, *Journal of Electroanalytical Chemistry* 581 (2005) 206.
- [20] J.W. Guo, T.S. Zhao, J. Prabhuram, R. Chen, C.W. Wong, *Journal of Power Sources* 156 (2006) 345.
- [21] N. Tsiouvaras, M.V. Martinez-Huerta, R. Moliner, M.J. Lazaro, J.L. Rodriguez, E. Pastor, M.A. Pena, J.L.G. Fierro, *Journal of Power Sources* 186 (2009) 299.
- [22] Z. Jusys, T.J. Schmidt, L. Dubau, K. Lasch, L. Jorissen, J. Garcke, R.J. Behm, *Journal of Power Sources* 105 (2002) 297.
- [23] X.Z. Cui, F.M. Cui, Q.J. He, L.M. Guo, M.L. Ruan, J.L. Shi, *Fuel* 89 (2010) 372.
- [24] J.L. Ye, J.G. Liu, Z.G. Zou, J. Gu, T. Yu, *Journal of Power Sources* 195 (2010) 2633.
- [25] X.Z. Cui, L.M. Guo, F.M. Cui, Q.J. He, J.L. Shi, *The Journal of Physical Chemistry C* 113 (2009) 4134.
- [26] K.Y. Tsang, T.C. Lee, J.W. Ren, K.Y. Chan, H.Z. Wang, H.T. Wang, *Journal of Experimental Nanoscience* 1 (2006) 113.
- [27] S. Jayaraman, T.F. Jaramillo, S.H. Baeck, E.W. McFarland, *The Journal of Physical Chemistry B* 109 (2005) 22958.
- [28] B. Rajesh, V. Karthik, S. Karthikeyan, K.R. Thampi, J.M. Bonard, B. Viswanathan, *Fuel* 81 (2002) 2177.
- [29] B.S.T. Hobbs, A.C.C. Tseung, *Nature* 222 (1969) 556.
- [30] A.C.C. Tseung, K.Y. Chen, *Catalysis Today* 38 (1997) 439.
- [31] A.C.C. Tseung, B.S. Hobbs, *Journal of Electrochemical Society* 117 (1970) C241.
- [32] B.S. Hobbs, A.C.C. Tseung, *Journal of Electrochemical Society* 122 (1975) 1174.
- [33] F. Micoud, F. Maillard, A. Gourgaud, M. Chatenet, *Electrochemistry Communications* 11 (2009) 651.
- [34] K.W. Park, J.H. Choi, K.S. Ahn, Y.E. Sung, *The Journal of Physical Chemistry B* 108 (2004), 108, 5989.
- [35] P.J. Barczuk, H. Tsuchiya, J.M. Macak, P. Schmuki, D. Szymanska, O. Makowski, K. Miecznikowski, P.J. Kulesza, *Electrochemical and Solid-State Letters* 9 (2006) E13.
- [36] B.S. Hobbs, A.C.C. Tseung, *Journal of Electrochemical Society* 119 (1972) 580.
- [37] B.S. Hobbs, A.C.C. Tseung, *Journal of Electrochemical Society* 120 (1973) 766.
- [38] A.C.C. Tseung, P.K. Shen, K.Y. Chen, *Journal of Power Sources* 61 (1996) 223.
- [39] F. Micoud, F. Maillard, A. Bonnefont, N. Job, M. Chatenet, *Physical Chemistry Chemical Physics* 12 (2010) 1182.
- [40] F. Maillard, E. Peyrelade, Y. Soldo-Olivier, M. Chatenet, E. Chainet, R. Faure, *Electrochimica Acta* 52 (2007) 1958.
- [41] X.Z. Cui, J.L. Shi, H.R. Chen, L.X. Zhang, L.M. Guo, J.H. Gao, J.B. Li, *The Journal of Physical Chemistry B* 112 (2008) 12024.
- [42] Z.G. Zhao, M. Miyauchi, *Angewandte Chemie International Edition* 47 (2008) 7051.
- [43] J. Rajeswari, B. Viswanathan, T.K. Varadarajan, *Material Chemistry and Physics* 106 (2007) 168.
- [44] X. Zhang, K.Y. Chan, J.K. You, Z.G. Lin, A.C.C. Tseung, *Journal of Electroanalytical Chemistry* 430 (1997) 147.
- [45] S.H. Lee, R. Deshpande, P.A. Parilla, K.M. Jones, B. To, A.H. Mahan, A.C. Dillon, *Advanced Materials* 18 (2006) 763.
- [46] C.M. White, J.S. Jang, S.H. Lee, J. Pankow, A.C. Dillon, *Electrochemical and Solid-State Letters* 13 (2010) B120.
- [47] L.F. Xiong, T. He, *Chemistry of Materials* 18 (2006) 2211.
- [48] S. Fardindoost, A.I. Zad, F. Rahimi, R. Ghasempour, *International Journal of Hydrogen Energy* 35 (2010) 854.
- [49] A. Phuruangrat, D.J. Ham, S.J. Hong, S. Thongtem, J.S. Lee, *Journal of Materials Chemistry* 20 (2010) 1683.
- [50] D. Tanaka, Y. Oaki, H. Imai, *Chemical Communications* 46 (2010) 5286.
- [51] M.B. Mohamed, K.M. Abouzeid, V. Abdelsayed, A.A. Aljarash, M.S. El-Shall, *ACS Nano* 4 (2010) 2766.
- [52] M. Tsuji, N. Miyamae, K. Matsumoto, S. Hikino, T. Tsuji, *Chemistry Letters* 34 (2005) 1518.
- [53] P.S.S. Prasad, N. Lingaiah, S. Chandrasekhar, K.S.R. Rao, P.K. Rao, K.V. Raghavan, F.J. Berry, L.E. Smart, *Catalysis Letters* 66 (2000) 201.
- [54] D.L. Boxall, C.M. Lukehart, *Chemistry of Materials* 13 (2001) 806.
- [55] Z.H. Liang, Y.J. Zhu, *Chemistry Letters* 33 (2004) 1314.
- [56] S.C. Padmanabhan, D. Ledwith, S.C. Pillai, D.E. McCormack, J.M. Kelly, *Journal of Materials Chemistry* 19 (2009) 9250.
- [57] C.L. Green, A. Kucernak, *The Journal of Physical Chemistry B* 106 (2002) 11446.
- [58] M. DeBlois, J. Lessard, G. Jerkiewicz, *Electrochimica Acta* 50 (2005) 3517.
- [59] A. Essalik, K. Amouzegar, O. Savadogo, *Journal of Applied Electrochemistry* 25 (1995) 404.
- [60] R. Ganesan, J.S. Lee, *Journal of Power Sources* 157 (2006) 217.
- [61] K.Y. Chen, Z. Sun, A.C.C. Tseung, *Electrochemical and Solid-State Letters* 3 (2000) 10.
- [62] Z. Sun, H.C. Chiu, A.C.C. Tseung, *Electrochemical and Solid-State Letters* 4 (2001) E9.
- [63] L.X. Yang, C. Bock, B. MacDougall, J. Park, *Journal of Applied Electrochemistry* 34 (2004) 427.
- [64] P.J. Kulesza, L.R. Faulkner, *Journal of Electroanalytical Chemistry* 259 (1989) 81.